Iowa State University

From the SelectedWorks of Eric W. Cochran

December, 2006

Effect of chain architecture and surface energies on the ordering behavior of lamellar and cylinder forming block copolymers

V. Khanna
Eric W. Cochran
A. Hexemer
G. E. Stein
G. H. Fredrickson, et al.

Available at: https://works.bepress.com/eric_cochran/14/

bepress™

Effect of Chain Architecture and Surface Energies on the Ordering Behavior of Lamellar and Cylinder Forming Block Copolymers

V. Khanna,[†] E. W. Cochran,[†] A. Hexemer,[†] G. E. Stein,[‡] G. H. Fredrickson,[†,‡] E. J. Kramer,*[,†,‡] X. Li,[§] J. Wang,[§] and S. F. Hahn[⊥]

Department of Materials, University of California, Santa Barbara, California 93106; Department of Chemical Engineering, University of California, Santa Barbara, California 93106; Advanced Photon Source, Argonne National Laboratory, Illinois 60439; and Performance Plastics and Chemicals, The Dow Chemical Company, Freeport, Texas 77541

Received April 26, 2006; Revised Manuscript Received August 22, 2006

ABSTRACT: We investigate the effect of surface energy and chain architecture on the orientation of microdomains in relatively thick films (600−800 nm) of lamellar and cylindrical block copolymers of poly(cyclohexylethylene) (C) and poly(ethylene) (E). The E block has 26 ethyl branches per 1000 backbone carbon atoms. Melt surface energies of the C and E blocks are 22.3 and 20.9 mJ/m^2, respectively. Grazing-incidence small-angle X-ray scattering (GISAXS), scanning force microscopy (SFM), and cross-sectional transmission electron microscopy (TEM) show that cylindrical and lamellar CEC triblock copolymers orient their microdomains normal to the surface throughout the film thickness. However, a lamellar CE diblock copolymer prefers a parallel orientation of the lamellae relative to the surface with an E surface layer. Moreover, a cylindrical CEBC triblock copolymer where the EB block has 125 ethyl branches per 1000 backbone carbon atoms leads to EB cylinder domains that always orient parallel to the surface. In this case the lower surface energy EB block dominates the surface. Calculations using self-consistent-field theory allow us to interpret the experimental results in terms of the entropic cost of forming a wetting layer comprised entirely of looping blocks. Thus, in triblock copolymers, parallel orientations are only stabilized when the midblock has the lower surface energy, and the difference in surface energies of the two blocks is large enough to compensate for this conformational penalty, which is absent in diblock copolymers.

Introduction

Block copolymers (BCPs) are composed of polymerized sequences or blocks of chemically distinct repeat units. The linear AB diblock is the simplest block copolymer architecture, consisting of a block of type A monomers covalently bonded to a block of type B monomers. By coupling additional A or B blocks to this simple architecture, multiblock copolymers can be obtained. If the chemically distinct blocks are immiscible, then excess free energy contributions are present that discourage mixing. However, in a block copolymer melt, these thermodynamic forces that drive separation are balanced by entropic constraints on the long chain molecules that arise from block connectivity. The morphology of the microphase separated structure depends on three parameters: (1) the Flory chi (χ) parameter between the two monomers, (2) the overall degree of polymerization N, and (3) the composition of the block copolymer f (volume fraction of A segments). Since χ varies inversely with temperature, above the order−disorder transition (ODT) temperature, the block copolymer is a disordered miscible melt. Below the ODT spherical, cylindrical, lamellar, and the gyroid morphologies with characteristic dimensions of the order of tens of nanometers can be observed.[1−3]

Because of this ability to self-assemble into nanoscale morphologies, block copolymers are versatile material candidates for a myriad of applications as bulk materials and in thin film geometries. In recent years, block copolymer thin films have been used as templates for the production of nanostructures and in nanoscale lithography. However, proper design and engineering of these materials is essential to ensure that such applications can be realized. In thin film applications, especially, control over the orientation of the nanodomains over macroscopic length scales is critical. A recent review of block copolymer thin films for patterning applications gives a comprehensive coverage of the topic.[4]

When a block copolymer is confined in a thin film geometry, the orientation of the microdomains is determined by the preferential wetting of top and bottom surfaces by the two blocks. This wetting, in turn, is determined by the surface energies of the two blocks at the interfaces. A number of techniques have been developed to tune the wettability of block copolymers on different surfaces and, hence, control the orientation of the microdomains in thin films.[5−9]

In this study we investigate the effects of surface energy, morphology, and architecture on the orientation of microdomains in block copolymer films. Poly(cyclohexylethylene) (PCHE) is a glassy amorphous polymer with excellent optical and thermal properties but an undesirable brittleness due to its high entanglement molecular weight (∼49 000 g/mol).[13] Block copolymers of PCHE and ductile poly(ethylene) (PE) can circumvent this undesirable brittleness. The thermodynamic,[14,15] viscoelastic,[16−18] and mechanical properties[19−21] of this block system have been studied extensively in previous works in both thin film and bulk geometries. Experiments on thin films of the cylindrical PCHE−PE−PCHE triblock copolymers (PE cylinders) showed that the microdomains preferred to orient themselves perpendicular to the interfaces,[19,20] a behavior that is not generally observed in block copolymers without the application of an external field (electric[5−7,10] or shear[11,12]) or surface modification.[5−9] The aim

[†] Department of Materials, UC Santa Barbara.
[‡] Department of Chemical Engineering, UC Santa Barbara.
[§] Argonne National Laboratory.
[⊥] The Dow Chemical Company.
* To whom correspondence should be addressed: e-mail edkramer@mrl.ucsb.edu; Tel (805) 893-4999.

10.1021/ma0609228 CCC: $33.50 © 2006 American Chemical Society
Published on Web 12/02/2006

Table 1. Molecular Weight, Composition, and Block Lengths of CE and CEC Block Copolymers

polymer	chain architecture	M_w (g/mol)	f_{PE} (wt %)	PCHE block (g/mol)	PE block (g/mol)	% 1,2 addition
$CE_{22.48.10}$	diblock	22 000	48	11 400	10 600	10
$CEC_{45.48.10}$	triblock	45 000	48	11 250	22 500	10
$CEC_{40.25.10}$	triblock	40 000	25	15 000	10 000	10
$CEC_{50.24.10}$	triblock	50 000	25	18 750	12 500	10
$CEBC_{60.25.40}$	triblock	60 000	25	22 500	15 000	40

of this work is to understand this peculiar behavior in both cylindrical and lamellar systems. The ordering behavior of a lamellar diblock copolymer is compared with that of a lamellar triblock copolymer to understand the effect of chain architecture. Additionally, the influence of surface energy is investigated by varying the ethyl branch content of the PE block. Transmission electron microscopy (TEM) and scanning force microscopy (SFM) images are complemented with small-angle X-ray scattering (SAXS) and grazing-incidence small-angle X-ray scattering (GISAXS)[22] measurements to obtain a complete picture of the morphology and orientation of the microdomains in the films.

Experiments and Theory

Materials and Thin Film Preparation. The poly(cyclohexylethylene)−poly(ethylene) block copolymers were synthesized at the Dow Chemical Co. The synthesis involved heterogeneous catalytic hydrogenation of polystyrene−polybutadiene (PS−PB) block copolymer precursors.[23] After hydrogenation, the PE blocks contained an average of 26 ethyl branches per 1000 backbone carbons. This was due to the 10% 1,2 monomer addition in the PB block (as determined by ^{1}H NMR analysis of the polymer prior to hydrogenation). However, one sample (entry 5 in Table 1) contains, on average, 1 ethyl branch per 8 backbone carbons due to the 40% 1,2 monomer addition in the PB block. In this study, the block copolymers had a poly(ethylene) weight fraction of 0.25 for the cylindrical systems and 0.48 for the lamellar systems. For the sake of convenience, a nomenclature is adopted for the different block copolymers where the C refers to the poly(cyclohexylethylene) block and E corresponds to the poly(ethylene) block. Hence, CE stands for a diblock copolymer and CEC stands for a triblock copolymer with a poly(ethylene) midblock. The names are followed by a six-digit number subscript. The first two digits indicate the M_w in kg/mol, the next two give the percentage weight fraction of poly(ethylene) in the block copolymer, and the last two indicate the percentage amount of 1,2 monomer addition in the poly(butadiene) precursor. As an example, $CEC_{40.25.10}$ is a 40 kg/mol triblock copolymer containing 25% poly(ethylene) and synthesized with a PB block precursor containing 10% 1,2 monomer addition. The molecular weights and composition of the block copolymers used in this study are listed in Table 1.

Uniform thin films of the block copolymer were spun-cast from hot decahydronaphthalene solutions (∼120 °C) on hot substrates at 2500 rpm for 40 s. For TEM and SFM samples, NaCl and Si wafers were used for substrates, respectively. For GISAXS measurements, 2 in. diameter Si wafers were used as substrates. The wafers were cleaned in piranha solution (H_2SO_4:H_2O_2 = 3:1 volume ratios) for 30 min, and a 2−3 nm thick native oxide layer was allowed to regrow. During spin-casting, the temperature of the substrate was maintained at 120 °C using an IR lamp with a voltage regulator. The resulting films were about 0.6 μm thick. For transmission SAXS measurements, bulk pieces of the block copolymers were used. Bulk polymer was pressed into 1 mm diameter and about 0.1 mm thick pellets using a hot press. The pressing temperature was about 160 °C. Subsequently, the pellets were annealed at the same temperature for the same time as the corresponding films. The annealing temperatures and times for the block copolymers are shown in Table 2. The annealing was done under a vacuum of about 10^{-8} Torr. The annealing temperatures were chosen such that they were sufficiently above the glass transition temperature of the glassy PCHE block (145 °C) but below the ODT of the block copolymers, which ensures that the block copolymer is well segregated before the glassy matrix vitrifies. The ODT of all the block copolymers under investigation was greater than 260 °C, as determined by dynamic mechanical analysis. The films were allowed to cool to the T_g of the glassy block at about 1.5 °C/min, below which they were quenched to room temperature.

Table 2. Annealing Temperatures and Time for the CE and CEC Block Copolymers

polymer	annealing temp (°C)	annealing time (days)
$CE_{22.48.10}$	220	3
$CEC_{45.48.10}$	220	3
$CEC_{40.25.10}$	220	3
$CEC_{50.24.10}$	220	3
$CEC_{60.25.40}$	220	4

Scanning Force Microscopy (SFM). To characterize the domain structures of the microphase-separated block copolymers, scanning force microscopy measurements were performed using a Digital Instruments Dimension 3000 and a Digital Instruments Nanoscope III. The microscopes were operated in tapping mode. The mechanical contrast between the glassy PCHE and softer PE domains enables the imaging of the microphase-separated domains of the polymer films.[24]

Transmission Electron Microscopy (TEM). Cross-sectional TEM of the thin films was done in order to characterize the orientation of the microdomains. The films were floated off the NaCl substrates onto the surface of a water bath and picked up on epoxy substrates. The films were then stained in RuO_4 vapor (0.5% RuO_4 aqueous solution, Electron Microscopy Sciences) for 12−24 h. Different rates of diffusion of the RuO_4 stain in the amorphous PE regions, the PE crystals, and the glassy PCHE matrix enable the morphological contrast.[25] This was followed by capping of the films with another layer of epoxy. 100 nm thick cross sections of the films were microtomed at room temperature using a Leica Ultracut UCT ultramicrotome and a diamond knife. The cross sections were imaged using an FEI-T20 TEM operated at 200 keV.

Small-Angle X-ray Scattering. Transmission SAXS measurements were performed at room temperature on annealed bulk polymer pellets using copper Kα radiation (λ = 1.54 Å) from a Rigaku rotating anode generator. The radiation was monochromated using an Osmic Confocal Maxflux double focusing multilayer mirror. The sample-to-detector distance was about 1720 mm, and the data were collected using a Bruker HI-STAR multiwire area detector.

GISAXS Measurements. The GISAXS measurements were performed at XOR-sector 1 and XOR-sector 8 at the Advanced Photon Source at Argonne National Laboratory. Monochromatized X-ray beams of 12 keV (λ = 0.1042 nm) and 7.4 keV (λ = 0.1675 nm) were used. The sample-to-detector distance was 2680 and 2007 mm, respectively, for the two beamlines. The sample-to-detector distance was calibrated with silver behenate, which has a periodicity of 58.376 Å. A piece of lead was used as a beam stop. The incident angle α_i for the 12 keV beam was varied from 0.04° to 0.12°, which is above the critical angle of the block copolymer film (α_c = 0.1°) but below that of the silicon substrate. For the 7.4 keV beam (α_c = 0.16°), α_i was varied from 0.04° to 0.21°. The data were typically collected for 10−30 s exposure, depending on the beam intensity, and a sum of 5−10 exposure images was taken for analysis. The images obtained were 2048 pixels × 2048 pixels in 16 bit TIFF format. Each pixel was 79 μm × 79 μm.

Surface Energy Measurements. The homopolymers used for surface energy measurements were poly(cyclohexylethylene), poly(ethylene), and poly(ethylene-*co*-butylene). Dow Chemical provided

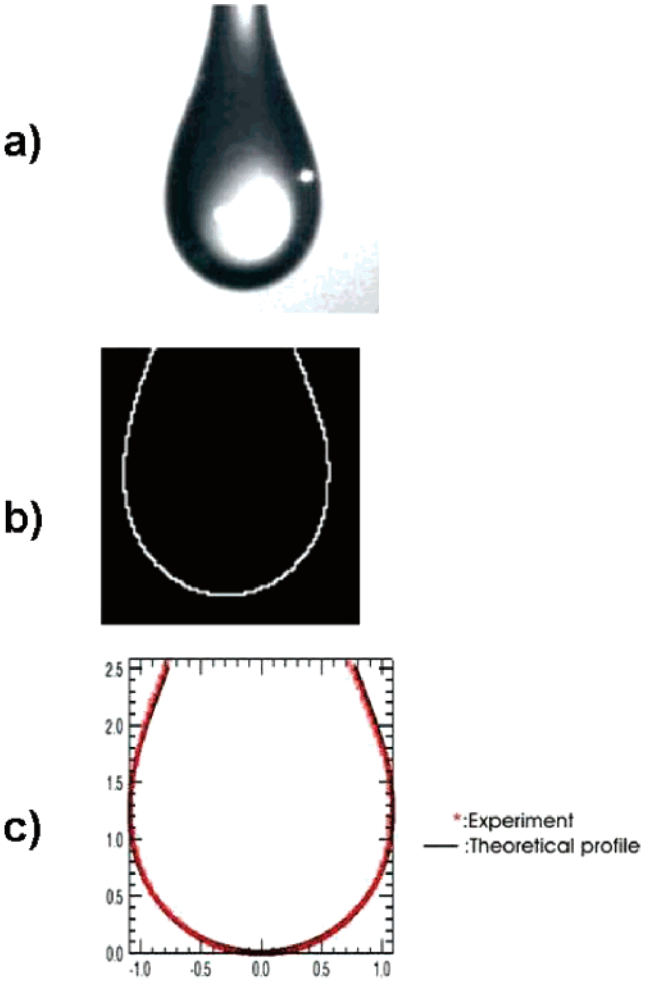

Figure 1. (a) Typical pendant drop digitized image, (b) after edge detection, and (c) superposition of the experimental profile (*) and the theoretical profile (—).

us with the PCHE and P-EB homopolymer. For PCHE, the M_n was equal to 129 000 g/mol and the M_w was equal to 283 000 g/mol. The P-EB homopolymer had an M_w of 53 300 g/mol and a PDI of 1.16. It was synthesized by the hydrogenation of a PB precursor made with 44% 1,2 monomer addition. The resulting P-EB polymer contained about 130 ethyl branches per 1000 backbone carbons. For the PE homopolymer, a 70 μm thick film was obtained from Exxon having an M_n equal to 31 700 g/mol and an M_w equal to 68 600 g/mol.[26] The polymer contained 25 ethyl branches per 1000 backbone carbons, which is comparable to the 26 ethyl branches per 1000 backbone carbons in the E blocks of the present study. The measurements were made using the pendant drop method which involves the determination of the profile of the molten polymer drop using digital imaging and shape analysis.[28,29] The drop profile depends on the balance of gravitational and surface forces. The surface tension can be determined using eq 1:

$$\gamma = \frac{a^2 g \Delta\rho}{B} \tag{1}$$

where g is the acceleration due to gravity, $\Delta\rho$ is the density difference between the polymer and the surrounding medium, i.e., vacuum for our experiments, a is the radius of curvature of the drop, and B is a dimensionless quantity that depends on the shape of the drop. Figure 1a−c shows a typical sequence of steps for inferring the surface energies. The algorithm for extracting the interfacial tension from the drop profile involves three major steps: (1) formation of the drop and capture and digitization of the image, (2) extraction and smoothing of the drop contour and determination of the radius of curvature a, and (3) shape comparison of the experimental and the theoretical drop profile to determine B. The experimental drop profile was obtained by heating a bulk piece of the polymer suspended from the roof of a vacuum oven (~1 mbar) to the required test temperature. After the polymer drop reached thermal and mechanical equilibrium, drop images were taken at regular intervals. For the shape comparison, the theoretical drop profile is obtained by solving the Bashforth and Adams equation.[27]

Self-Consistent-Field Theory Calculations. We use self-consistent-field theory (SCFT)[30−35] calculations to aid the interpretation of our experimental data. SCFT, which has been shown to encapsulate many important features of the equilibrium behavior of block copolymer melts, reduces the problem of calculating the partition function for a collection of interacting chains to that of finding a constrained partition function $q(\mathbf{r},s)$ for a single polymer chain of contour length s with its end segment at position in an inhomogeneous chemical potential field. Matsen[34] first applied the SCFT of Helfand[35] to thin films of symmetric AB diblock copolymer lamellae; we adopt a similar approach here to investigate the influence of chain architecture on the stability of the parallel and perpendicular orientations of lamellae and hexagonally packed cylinders as a function of surface interactions.

Our approach to SCFT of thin films is to utilize a "masking" technique that confines the block copolymer between two surfaces by prescribing an interfacial density field (or "cavity" field), $\rho_W(\mathbf{r})$ (W stands for wall), that expels polymer through the imposition of a modified incompressibility constraint, $\rho_A(\mathbf{r}) + \rho_B(\mathbf{r}) + \rho_W(\mathbf{r}) = 1$. Here we employ normalized densities $\rho_i(\mathbf{r})$ that can be interpreted as volume fractions of species i. Regions for which $0 < \rho_W(\mathbf{r}) < 1$ represent overlap of the substrate (or air) with the polymer. The enthalpic interactions that arise from this overlap may be accounted through the introduction of quadratic terms of the form $\rho_i(\mathbf{r})\rho_W(\mathbf{r})\chi_{iW}$ to the standard field-theoretic Hamiltonian:

$$\frac{H}{nk_BT} = \frac{1}{V}\int d^3\mathbf{r}\,[\rho_A\rho_B\chi_{AB}N + \rho_A\rho_W\chi_{AW}N + \rho_B\rho_W\chi_{BW}N - \rho_A w_A - \rho_B w_B - p(1 - \rho_A - \rho_B - \rho_W)] - \ln Q \tag{2}$$

where n is the number of chains and Q is the partition function of a single chain experiencing chemical potential fields w_A and w_B. Here V represents the effective volume occupied by polymer species, i.e.

$$V = \int d^3\mathbf{r}\,(1 - \rho_W(\mathbf{r})) \tag{3}$$

Here and in subsequent equations it is convenient to express all lengths and volumes in units of R_g, the unperturbed radius of gyration of the block copolymer. The Flory parameter χ_{AB} controls the degree of incompatibility between A and B blocks, while χ_{AW} and χ_{BW} are dimensionless measures of the surface energies of the A and B blocks. Note that the case of $\chi_{AW} > 0$, $\chi_{BW} = 0$ corresponds to a B-attractive wall. The pressure field p enforces the local incompressibility condition, $\rho_A(\mathbf{r}) + \rho_B(\mathbf{r}) + \rho_W(\mathbf{r}) = 1$.

The choice of $\rho_W(\mathbf{r})$ determines the geometry of the film; here we consider a melt confined between two planar interfaces with normals directed along the x-axis:

$$\rho_W(\mathbf{r}) = \frac{1}{2}\left(1 + \tanh\left(4\,\frac{\frac{1}{2}(T + L_x) - |r_x - \frac{1}{2}L_x|}{t}\right) \times \tanh\left(4\,\frac{\frac{1}{2}(T + L_x) + |r_x - \frac{1}{2}L_x|}{t}\right)\right) \tag{4}$$

This expression, which is sketched in Figure 2, describes a planar cavity field centered at the yz-plane with an overall cavity thickness T. The projection of the position vector $\mathbf{r}$ along the x-axis is given by r_x, and t is the interfacial thickness of the transition from "inside" to "outside" the cavity field. Thus, a value of $r_x = {}^1/_2T$ may be viewed as the center of the polymer/substrate interface while $r_x =$

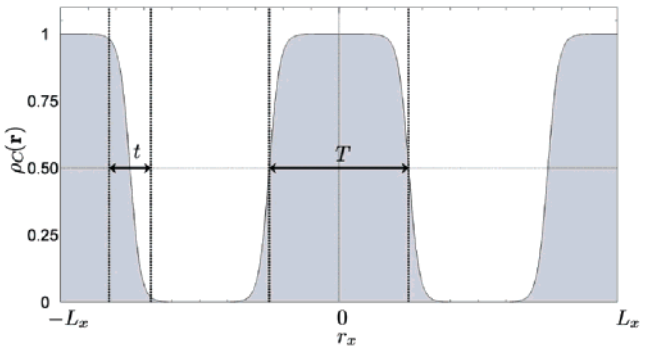

Figure 2. Film geometry corresponding to eq 4 showing the depth profile of the interfacial density field for two unit cells (two thin films). Here $t = 0.15L_x$ and $T = 0.5L_x$. Incompressibility renders the shaded regions inaccessible to the block copolymer. Surface interactions are manifested through the overlap region of width t where $0 \lesssim \rho_W(\mathbf{r}) \lesssim 1$.

$L_x - {}^1/_2T$ represents the center of the polymer/air interface. Equation 4 asymptotically approaches values of 0 and 1, and so the "beginning" and "end" of the polymer/cavity regions must be defined; the quantity $4/t$ serves this purpose, so that the transition from $\rho_W(\mathbf{r}) = 0.02$ (mostly polymer) to $\rho_W(\mathbf{r}) = 0.98$ (mostly cavity) occurs over a thickness of t. The functional form is particularly convenient for the use of pseudo-spectral numerical methods with periodic boundary conditions.

In order for $\rho_W(\mathbf{r})$ to represent confining surfaces, the interfacial region should be small, i.e., $t < 1$ should hold; we have found that all values of t for $t < {}^1/_2$ lead to qualitatively identical results. For $t \ll {}^1/_2$ the interface is exceedingly sharp, requiring a computationally expensive degree of spatial resolution and slowing the convergence of the SCFT equations. Values of T should be chosen to prevent the overlap of the two interfaces; we use a choice of $t = {}^1/_2$ and $T = 1$. The effective thickness of the simulation volume available to the polymer is $d = L_x - T$.

For a diblock copolymer with a volume fraction f of A blocks, $q(\mathbf{r},s)$ satisfies the modified diffusion equation (MDE)

$$\frac{\partial q(\mathbf{r},s)}{\partial s} = \nabla^2 q(\mathbf{r},s) - w_i(\mathbf{r})\, q(\mathbf{r},s) \tag{5}$$

subject to the initial condition $q(\mathbf{r},0) = 1$, where $i = A$ for $s < f$ and $i = B$ for $s > f$. The local density operators $\rho_A(\mathbf{r})$ and $\rho_B(\mathbf{r})$ are

$$\rho_A(\mathbf{r}) = \frac{1}{Q}\int_0^f \mathrm{d}s\; q(\mathbf{r},s)\, q^\dagger(\mathbf{r},s) \tag{6}$$

$$\rho_B(\mathbf{r}) = \frac{1}{Q}\int_f^1 \mathrm{d}s\; q(\mathbf{r},s)\, q^\dagger(\mathbf{r},s) \tag{7}$$

where $q^\dagger(\mathbf{r},s)$ is the solution to eq 9 subject to $q^\dagger(\mathbf{r},1) = 1$. Q is the single-chain partition function whose relationship to $q(\mathbf{r},s)$ is

$$Q = \frac{1}{V}\int \mathrm{d}\mathbf{r}\; q(\mathbf{r},1) \tag{8}$$

At a saddle point these fields must satisfy

$$w_A = \rho_B\chi_{AB}N + \rho_W\chi_{AW}N + p \tag{9}$$

$$w_B = \rho_A\chi_{AW}N + \rho_W\chi_{BW}N + p \tag{10}$$

$$\rho_A(\mathbf{r}) + \rho_B(\mathbf{r}) + \rho_W(\mathbf{r}) = 1 \tag{11}$$

where ρ_A and ρ_B are obtained from eqs 10 and 11 and the pressure p is chosen to satisfy eq 15. At a saddle point, for a B-attractive wall ($\chi_{BW} = 0$, $\chi_{AW} > 0$) the free energy per chain may be calculated as

$$\frac{F}{nk_BT} = \frac{1}{V}\int \mathrm{d}\mathbf{r}\; (\rho_A\rho_B\chi_{AB}N + \rho_A\rho_W\chi_{AW}N - \rho_A w_A - \rho_B w_B - p(1 - \rho_A - \rho_B - \rho_W)) - \ln Q \tag{12}$$

The extension to ABA triblock copolymers is straightforward. The MDE was solved using a fourth-order backward difference formula (BDF):[37]

$$\frac{25}{12}q_{n+1} - 4q_n + 3q_{n-1} - \frac{4}{3}q_{n-2} + \frac{1}{4}q_{n-3} = \Delta s[\nabla^2 q_{n+1} - w(\mathbf{r})(4q_n - 6q_{n-1} + 4q_{n-2} - q_{n-3})] \tag{13}$$

where Δs is the step size along the chain contour. Saddle-point configurations of the pressure field were calculated using a semiimplicit relaxation scheme devised by Cenicernos and Fredrickson,[38] while explicit Euler relaxation was used to optimize the mean-field chemical potential fields w_A and w_B. The box shape parameters in the transverse directions, L_y and L_z, were continuously adjusted toward optimal values for a single unit cell by calculating the local microscopic stress using an explicit algorithm.[39] The BDF method for solving the MDE and box shape optimization techniques will be discussed in greater detail in a forthcoming publication.[40]

Our calculations included the AB and symmetric ABA architectures with $f_B = 0.5$ and $f_B = 0.25$, for which lamellae and cylinders, respectively, are the stable phases in the bulk. The excess surface energy per unit area (surface tension) is proportional to $(F - F_B)d/nk_BT$, where F/nk_BT is the (intensive) free energy of the confined system and F_B/nk_BT is the corresponding quantity in the bulk. The optimal film thicknesses of parallel orientations are indicated by the minima in $(F - F_B)d$ vs d. The experimental films considered in this work are too thick ($\approx xR_g$) for calculations using the same thickness to be computationally tractable on a reasonable time scale. Instead, we gradually increased d until $(\partial(F - F_B)d/nk_BT)/\partial d \approx 0$, i.e., into the regime where the thickness is irrelevant. A summary of the parameters used in these calculations appears in Table 3. Note that the nomenclature of A and B blocks in the calculations corresponds to the C and E blocks in the experimental results.

Table 3. Summary of Parameters Used for Thin Film SCFT Calculations

polymer	f_A	f_B	χ_{AB}	$d_{\|}$, R_g[a]	$d_\perp$, R_g[b]	Δx_{max}, R_g[c]	Δs
AB	0.5	0.5	20	8.1	18	0.1	0.01
ABA	0.5	0.5	34	5.9	12	0.1	0.01
ABA	0.75	0.25	40	4.9	12	0.1	0.01

[a] Effective film thickness used for parallel orientation; corresponds to an optimal film thickness. [b] Effective film thickness used for perpendicular orientation. [c] Maximum mesh size.

Results

Surface Energy Measurements. The surface energies of PCHE, PE, and P-EB in the melt were measured using the pendant drop method. The temperature of 220 °C was chosen for the measurements, which is also the annealing temperature for all the BCP films (Table 1). For the PCHE homopolymer, the time to reach thermal and mechanical equilibrium was substantially more than that of the PE and P-EB homopolymer. This was probably due to the high T_g and high M_w and hence the high viscosity of the polymer. The PCHE homopolymer was held at this temperature for 3 days until a suitable drop was obtained that did not seem to change shape over the next 24 h. For PE, the mechanical equilibrium was reached over 10 h, whereas for the P-EB homopolymer, the images were obtained after 3 h of heating. After superposing the theoretical drop profile on our experimental results, the value of B, the

Table 4. Polymer Melt Density, Radius of Curvature and Surface Energy at 220 °C

polymer	ρ (kg/m^3)	a (mm)	γ (mJ/m^2)
PEB	746.4	1.09	17.6
PE	741.6	1.1	20.9
PCHE	862.2	1.09	22.3

dimensionless shape factor, was obtained. To calculate γ from B (eq 3), the values of a, the radius of curvature at the apex of the drop, and ρ, the density of the polymers at 220 °C, were required. The value of a is obtained by fitting circles of different radii to the drop apex. The radius of the circle with the best fit is taken as the radius of curvature. The melt density of PE at 220 °C was obtained from the work of Richter et al.[16] Their work documents the melt densities of PE-2 (20 ethyl branches per 1000 backbone carbons) from 145 to 283 °C. A linear fit of the data gives us the value of the melt density of PE-2 at 220 °C. Since the PE in our work contains about 26 ethyl branches per 1000 backbone carbons (PE-2.6), we believe that the value is reasonable for our calculations. Using a linear extrapolation of the densities of P(EB)-14 (140 ethyl branches per 1000 backbone carbons) at 25 °C and P(EB)-11.7 (117 ethyl branches per 1000 backbone carbons) at 140 °C from the work of Fetters et al.,[41] a reasonable estimate of the density of P(EB)-12.5 (125 ethyl branches per 1000 backbone carbons) at 220 °C can be obtained. For PCHE, the value of melt densities at 160[17] and 187 °C[18] were obtained, and a linear extrapolation was done to obtain the value of the melt density at 220 °C.

Using eq 3, the values of a obtained from the drop images and the melt densities obtained above, the surface energies of PCHE, PE, and PEB at 220 °C can be calculated. The melt densities ρ, radius of curvature a, and surface energies γ of the three homopolymers are listed in Table 4. For the sake of comparison, using the Flory, Orwoll, and Vrij (FOV) equation of state theory, Dee and Sauer predicted the surface tension of linear PE (M_n = 28 000 g/mol) to be about 22 mJ/m^2 at 220 °C.[42]

Characterization of Block Copolymer Films. The following sections describe the morphological characterization of the block copolymer films used in the study. The block copolymers are listed in Table 1. Transmission electron microscopy (TEM) and scanning force microscopy along with grazing incidence small-angle X-ray scattering (GISAXS) results are reported.

CE$_{22.48.10}$. The CE diblock copolymer was annealed at 220 °C for 3 days. SFM images of the films surface show crystalline features in an amorphous matrix (Figure 3a) which indicate that the poly(ethylene) block covers the surface of the film. Transmission SAXS patterns give the position of the first-order peak at $q = 0.245$ nm^{-1}, which corresponds to a d spacing of 25.6 nm. Cross-sectional TEM of the film showed that the alternating lamellar sheets of the diblock copolymer architecture were aligned parallel to the film interfaces (Figure 3b). This orientation persisted throughout the film thickness after sufficient annealing. Hence, the diblock prefers to align itself parallel to the film interfaces with the poly(ethylene) block on the surface of the film.

CEC$_{45.48.10}$. The triblock copolymer film was annealed at 220 °C for 3 days. The block copolymer shows a lamellar morphology. SFM and cross-sectional TEM images of the films show that the lamellar sheets are oriented perpendicular to the plane of the film, and the orientation persists throughout the film thickness (Figure 4). Transmission SAXS diffraction patterns show that the first-order peak exists at $q^* = 0.245$ nm^{-1}, corresponding to a d spacing of 25.6 nm. Angle-resolved GISAXS measurements were carried out to obtain information about the microdomain orientation at different depths from the film surface. When the incident angle is below the critical angle

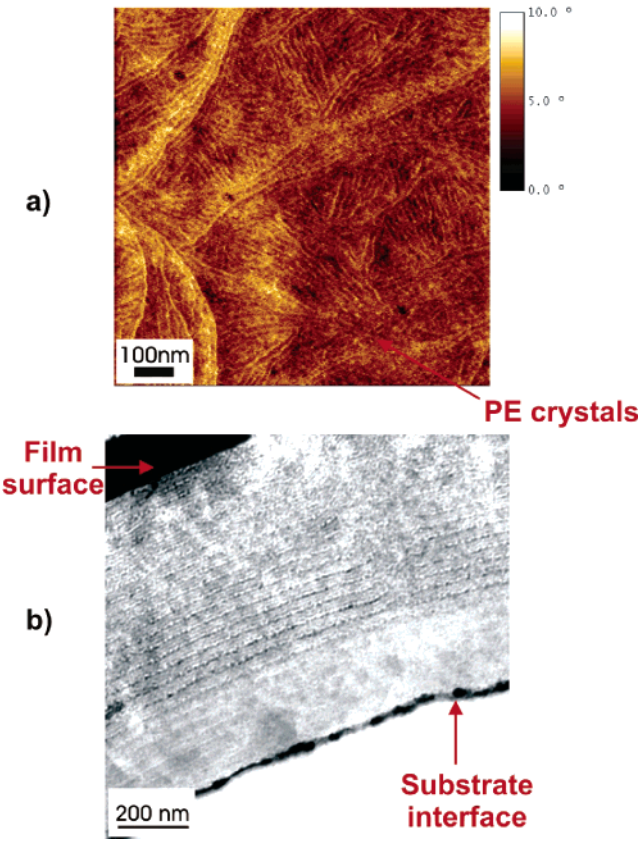

Figure 3. CE$_{22.48.10}$ annealed at 220 °C for 3 days: (a) Tapping mode SFM phase image; (b) cross-sectional TEM image.

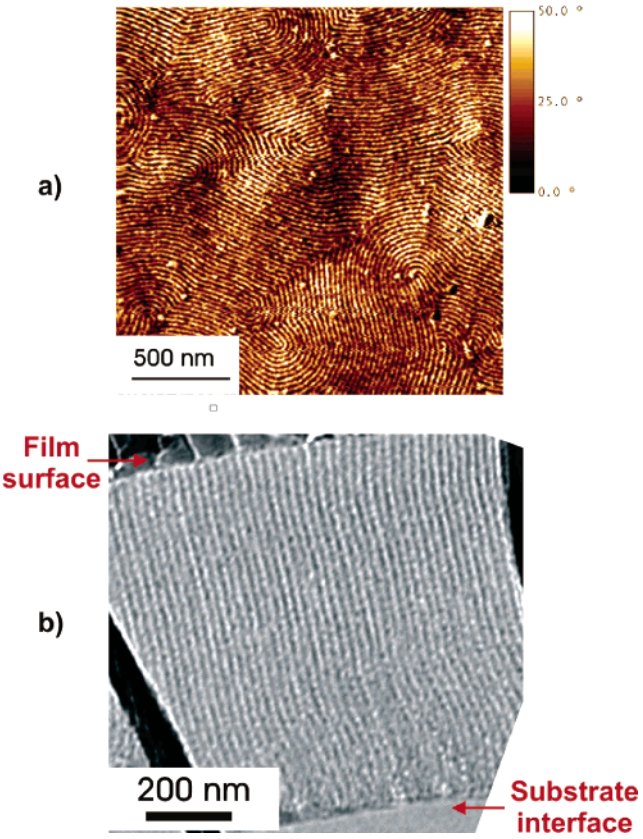

Figure 4. CEC$_{45.48.10}$ annealed at 220 °C for 3 days: (a) Tapping mode SFM phase image; (b) cross-sectional TEM image.

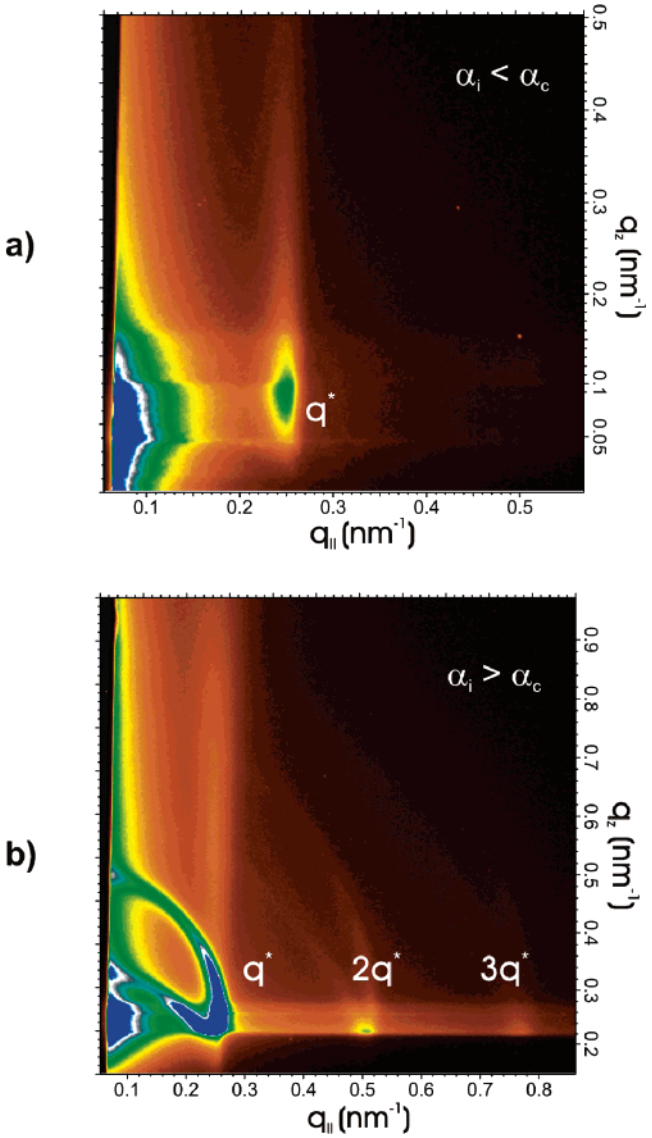

Figure 5. GISAXS pattern ($\lambda = 0.1675$ nm) at an incident angle of (a) 0.06° and (b) 0.21° of $CEC_{45.48.10}$ annealed at 220 °C for 3 days.

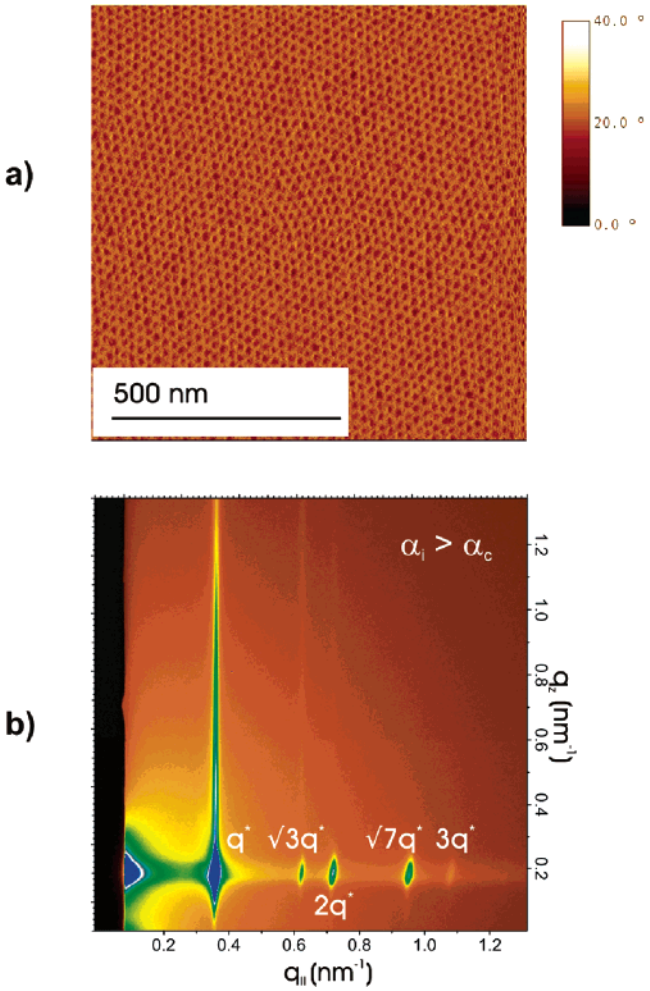

Figure 6. (a) Tapping mode SFM phase image. (b) GISAXS pattern at an incident angle of 0.12°, $\lambda = 0.1042$ nm, of $CEC_{40.25.10}$ annealed at 220 °C for 3 days.

of the polymer film ($\alpha_i = 0.06°$, $\lambda = 0.1675$ nm), the X-rays probe only the surface of the film. At incident angles greater than the critical angle of the polymer film but less than the critical angle of the substrate ($\alpha_i = 0.21°$, $\lambda = 0.1675$ nm), the X-rays probe the complete depth of the film. Below the critical angle of the film, the GISAXS pattern shows a single peak corresponding to the lamellar spacing for the block copolymer (Figure 5a). The peak occurs at $q_{||} = 0.253$ nm^{-1}, corresponding to a *d* spacing of 24.8 nm. The peak direction suggests that the lamellar sheets are oriented perpendicular to the film plane. However, at incidence angles above the critical angle, we see diffraction rings coexisting with the single diffraction peak where the relative peak positions are q^*, $2q^*$, and $3q^*$. This implies that in the bulk of the film some of the lamellar sheets are oriented randomly (Figure 5b) due to insufficient annealing time for the block copolymer film.

$CEC_{40.25.10}$ and $CEC_{50.24.10}$. The two triblock copolymer films were annealed at 220 °C for 3 days. The block copolymers show a cylindrical morphology with E cylinders embedded in a C matrix. From the SAXS patterns, the first-order peak occurs at 0.351 and 0.30 nm^{-1}, corresponding to a (10) plane spacing of 17.9 and 20.95 nm for the 40 and 50 kg/mol triblocks, respectively. SFM images show that the E cylinders are aligned perpendicular to the plane of the film (Figures 6a and 7a). Ruokolainen et al. have reported cross-sectional TEM images of the 50 kg/mol block copolymer in a previous work, which clearly show that the perpendicular orientation is present throughout the thickness of the film.[20]

The SFM and TEM results are clearly corroborated by the GISAXS measurements. For $CEC_{40.25.10}$, the in-plane diffraction pattern (constant q_z) of the block copolymer film shows several diffraction peaks where the relative peak positions or relative scattering vector lengths are q^*, $\sqrt{3}q^*$, $2q^*$, and $\sqrt{7}q^*$ (Figure 6b). The peaks and their relative positions indicate that the cylinders are oriented with their axes perpendicular to the film plane. No other peaks or rings are observed, and the out-of-plane intensity along q_z is due to the form factor of the cylinders that are standing up throughout the thickness of the film. The first-order peak is observed at $q_{||} = 0.36$ nm^{-1}, corresponding to a plane spacing of 17.45 nm, which is in good agreement with the SAXS results.

The $CEC_{50.24.10}$ films show a 2D diffraction pattern that is very similar to the lower M_w triblock (Figure 7b). However, weak diffraction rings are also observed along with the sharp diffraction peaks. The peaks suggest the predominance of the perpendicular orientation. The first-order peak is observed at 0.304 nm^{-1}, corresponding to a (10) plane spacing 20.7 nm, a result that is again corroborated by SAXS measurements. However, the presence of rings as well as the absence of strong higher order peaks suggests the presence of a small fraction of

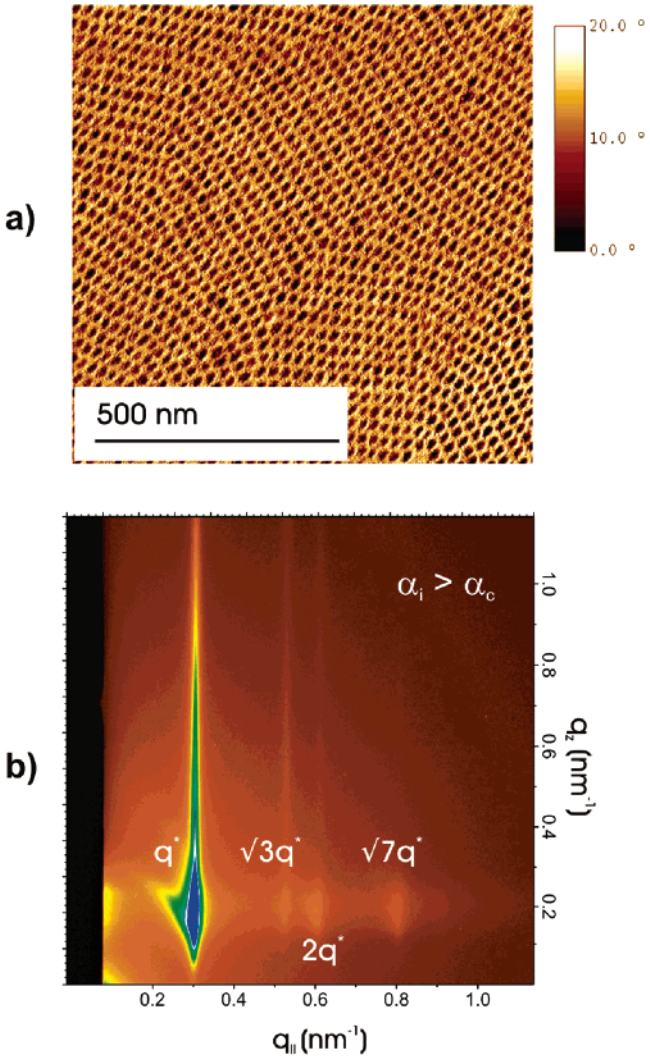

Figure 7. (a) Tapping mode SFM phase image. (b) GISAXS pattern at an incident angle of 0.12°, $\lambda = 0.1042$ nm, of $CEC_{50.24.10}$ annealed at 220 °C for 3 days.

randomly oriented microdomains and absence of long-range order due to trapped defects. These observations are in agreement with the SFM images which show poorer lateral order in the higher M_w triblock film, perhaps due to the low annealing temperature or insufficient annealing time.

CEBC$_{60.75.40}$. This particular triblock copolymer was different from the previous two in that the E block was made by hydrogenation of PB synthesized to produce 40% 1,2 monomer addition and 60% 1,4 monomer addition. The resultant E block has a much higher ethyl branch content of 1 ethyl branch per 8 backbone carbons as compared to the previous block copolymers and thus an ethylene−butylene architecture. The films were annealed at 220 °C for 4 days. SFM images show that the cylinders are oriented with their axes parallel to the film plane (Figure 8a,b). Transmission SAXS patterns give the first-order peak at $q = 0.316$ nm^{-1}, corresponding to a (10) plane spacing of 19.9 nm. However, a cross-sectional TEM image of the film shows that the parallel orientation persists only in the top few layers of the film, after which the cylinders orient with their axes perpendicular to the film plane (Figure 8c). The GISAXS patterns corroborate the TEM image. Two sharp peaks are observed along the $q_{||}$ direction at position labeled q_{par} and q_{per} in Figure 8b. These arise from the cylinders in the parallel and perpendicular orientations respectively with the expected ratio of q_{par} to q_{per} of $1:2/\sqrt{3}$. This corresponds to the inverse of the ratio between nearest-neighbor spacing (for cylinders parallel to the film plane) and close-packed plane spacing (for the perpendicular orientation) in a hexagonal arrangement. The first-order peak for the perpendicular orientation, i.e., q_{per}, occurs at 0.32 nm^{-1}, which corresponds to a (10) plane spacing of 19.6 nm, a result that is in good agreement with the transmission SAXS data.

SCFT Calculations. The SCFT results are shown in Figures 9 and 10 for the lamellar and cylindrical block copolymers, respectively. For the symmetric lamellar block copolymers, the excess free energy for the parallel and perpendicular configurations is shown as a function of $\chi_{AW}N$ for the AB diblock architecture (Figure 9a) and the ABA triblock architecture (Figure 9b). Note that W stands for the wall or interface. For the diblock copolymer, the perpendicular orientation is energetically favorable up to $\chi_{AW}N \sim 1$. For the neutral case ($\chi_{AW}N = 0$), the difference in the free energy between the parallel and perpendicular orientation is only about $0.1nk_BTR_g$. Further increase in $\chi_{AW}N$, i.e., the repulsion between the A block and the wall, stabilizes the parallel orientation with the lower γ B block on the surface. Hence, even for small differences in the surface energy of the two blocks, the B block will cover the surface and the lamellar sheets will order parallel to the film interfaces. For the triblock copolymer, three configurations are considered for the calculations. The parallel configurations with (1) end block A on the surface, (2) midblock B on the surface, and (3) the perpendicular configuration with both A and B on the surface. For the neutral case, i.e., when $\chi_{AW}N = 0$, the perpendicular configuration is the lowest free energy state, a result similar to what is obtained from calculations for the diblock architecture. However, the difference in energies between the parallel (midblock B on surface) and perpendicular orientations is $>1nk_BTR_g$, which is an order of magnitude higher than the difference for the diblock architecture. Moreover, contrary to what is observed for the diblock architecture, the perpendicular orientation is stable for the triblock architecture over a much larger range of $\chi_{AW}N$, and the crossover from perpendicular to parallel orientation occurs at $\chi_{AW}N \sim 12$. This suggests that even if the surface has a relatively strong repulsion for one block, the perpendicular orientation remains the lowest free energy state.

For the cylindrical triblock copolymer ABA, the excess free energy contributions are plotted as a function of $\chi_{AW}N$, the surface interaction of the end block A with the wall, for the two parallel orientations (A wetting the surface and B wetting the surface) and the perpendicular orientations (Figure 10). The crossover from perpendicular to parallel occurs at $\chi_{AW}N \sim 2$. This implies that the perpendicular orientation is favorable over a much smaller range of surface interaction difference for the cylindrical triblock as compared to the lamellar triblock. Note that for the neutral as well as positive values of $\chi_{AW}N$ the parallel orientation with the outer block A wetting the surface is never energetically favorable. The case where B wets the surface and the cylinders are oriented parallel to the interfaces is discussed in more detail in the following section.

Discussion

Typically, block copolymers with a lamellar or cylindrical morphology, when confined in relatively thick films, exhibit an orientation where the lamellae or cylinders are parallel to the film interfaces. The block with the lower surface energy forms a thin brush layer at the interfaces. However, a perpendicular orientation of the microdomains may be observed if the surface energies of the two blocks are closely matched.[44,45] We

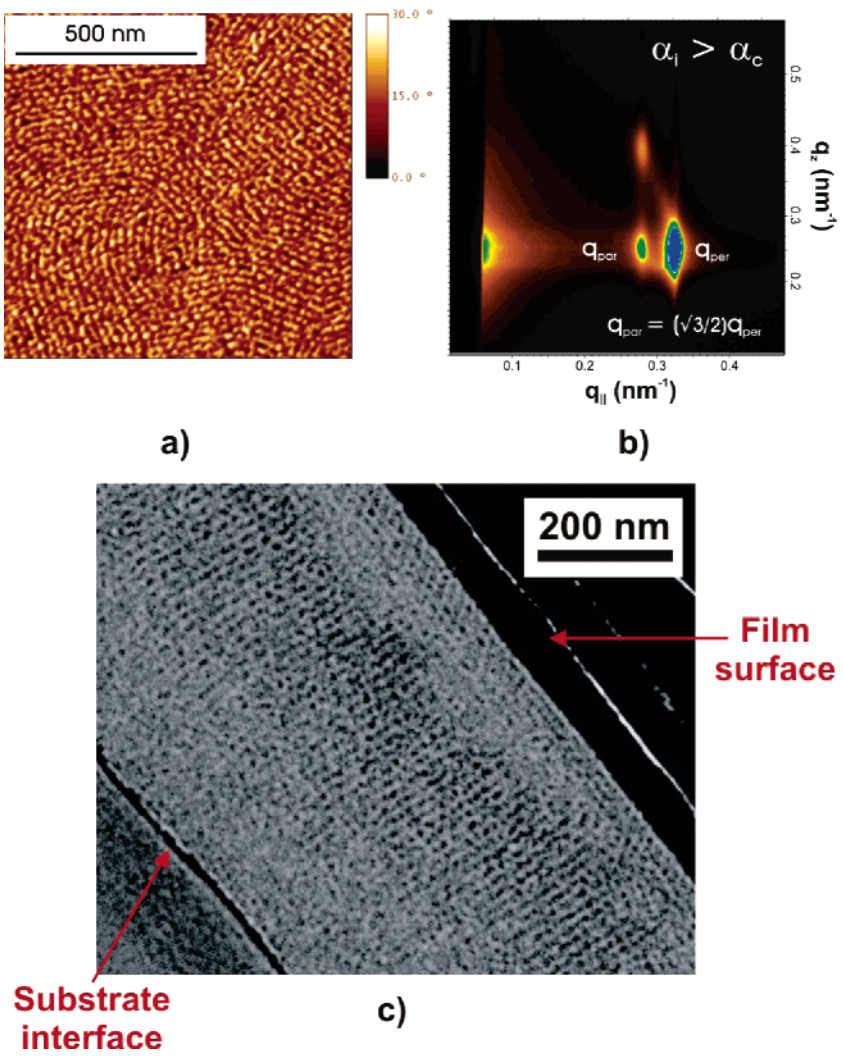

Figure 8. (a) Tapping mode SFM phase image. (b) GISAXS pattern at an incident angle of 0.21°, $\lambda = 0.1675$ nm. (c) Cross-sectional TEM image of $CEC_{60.24.40}$ annealed at 220 °C for 4 days. The E block contains about 1 ethyl branch per 8 backbone carbons due to the 40% 1,2 monomer addition in the PB precursor.

observe this atypical behavior in the poly(cyclohexylethylene)−poly(ethylene) system for both lamellar and cylindrical morphologies. The phenomena may be understood by considering the surface energy of C and E. Pendant drop measurements indicate that the surface energy of E is only slightly lower than that of C, which from an enthalpic standpoint means that an E wetting layer will slightly lower the internal energy, regardless of block architecture.

SCFT calculations for the lamellar block copolymers show that the perpendicular orientation for the triblock architecture is energetically more favorable over a larger range of $\chi_{AW}N$ when compared to the diblock architecture (Figure 9). Hence, for small differences in the surface energy of the two blocks, as is the case for PCHE and PE (Table 4), the parallel configuration is favored for the diblock architecture whereas the perpendicular orientation is energetically more desirable for the triblock architecture. This is also evident from the experimental results for $CE_{22.48.10}$ (Figure 3) and $CEC_{45.48.10}$ (Figure 4). The reasons for this behavior can be qualitatively understood if the configurations of the blocks for the two architectures are considered in the parallel and the perpendicular orientations.

For the lamellar triblock copolymer, a looping of the lower surface energy midblock is required in order for it to cover the air−film interface, as shown in Figure 11. The lamellar sheets will lie parallel to the interface if the entropy loss associated with this looping can be sufficiently compensated by a gain in surface energy due to the looped top layer. Ten Brinke and Hadziioannou[46] and Balsara et al.[47] examined the formation of micelles with poorly solvated looped coronal blocks (the end blocks B in BAB triblock copolymers) and estimated the entropy loss associated with this looping. Assuming weakly perturbed chains, they estimated the contribution per loop to the free energy by the expression

$$F_{loop} = \frac{1}{2}k_B T \ln(\pi\chi N_{PE}) \qquad (14)$$

De Jeu et al. used the expression to estimate the gain in surface energy in thin films of lamellar triblock copolymers.[48] In the context of our system, if this loss in entropy due to the looping of the lower surface energy midblock is less than the gain in surface energy written as $(\gamma_{PCHE} - \gamma_{PE})\sigma$, where σ is the surface area per chain, the sheets will align perpendicular to the film interface. Taking the value of $\chi_{PCHE-PE}$ from ref 14 and calculating σ from the density of the block copolymer and the lamellar period (~25 nm), it can be seen that if $\gamma_{PCHE} - \gamma_{PE} < 4.4$ mJ/m^2, the perpendicular orientation is favored since $\Delta\gamma$ is too small to compensate for the entropic penalty due to the midblock looping. From the surface energy measurements, this criterion is satisfied by the PCHE−PE system. However,

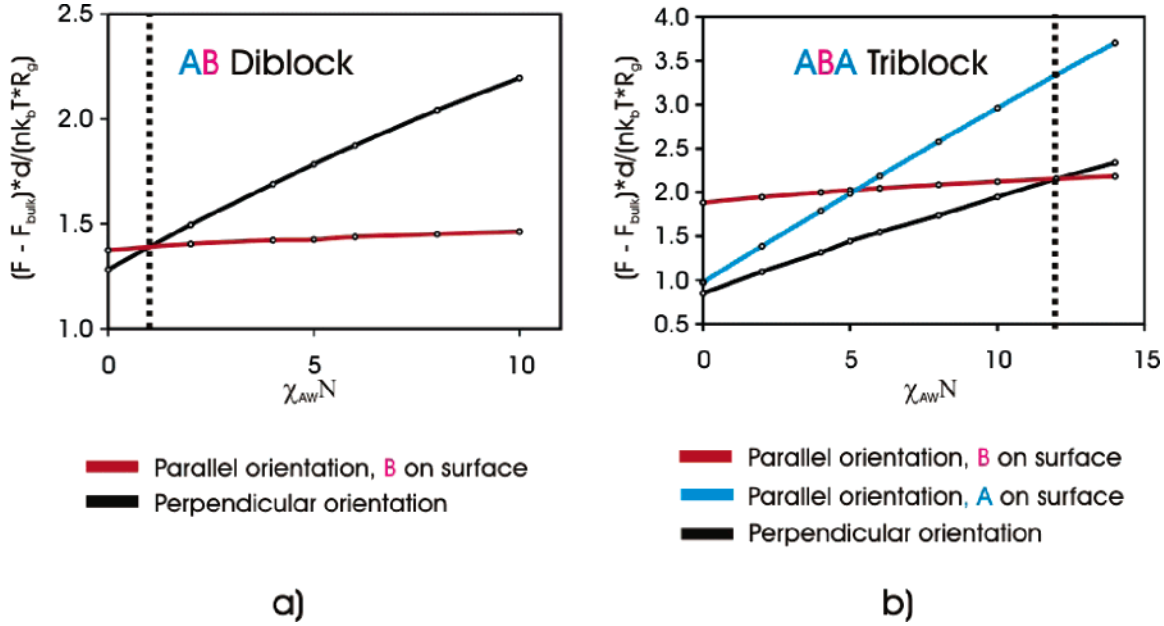

Figure 9. Self-consistent-field theory calculations for (a) 50/50 AB diblock copolymer and (b) 25/50/25 ABA triblock copolymer showing the excess free energy for different orientations as a function of $\chi_{AW}N$, which is a measure of the repulsion between the A block and the surface. The equilibrium morphology is lamellar, and d is the film thickness. The dotted line in both figures indicates the value of $\chi_{AW}N$ at which the parallel orientation (B block on the surface) becomes energetically more favorable than the perpendicular orientation.

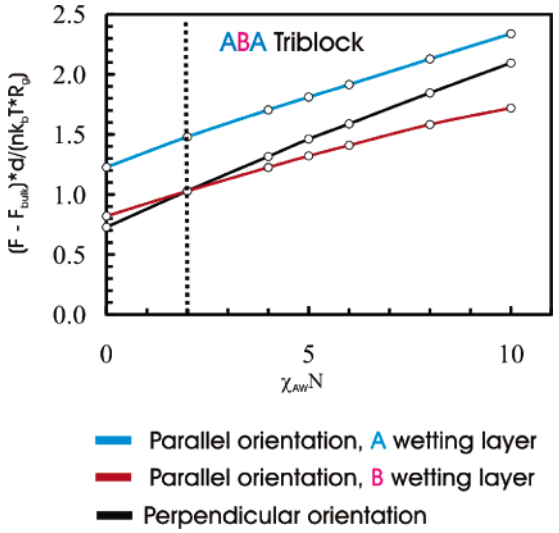

Figure 10. Self-consistent-field theory calculations for 37/25/38 ABA triblock copolymer showing the excess free energy for different orientations as a function of $\chi_{AW}N$. The equilibrium morphology is cylindrical. The dotted line indicates the value of $\chi_{AW}N$ at which the parallel orientation, with a B wetting layer, becomes energetically more favorable than the perpendicular orientation.

since no such looping constraint exists on the film surface for the diblock architecture (Figure 11), a parallel morphology is observed. While for thinner films, nonoptimal thickness has been shown to cause reorientation of the thin film morphology from parallel to perpendicular, this cannot be the case in our experiments. The thickness of the films under investigation is large (~600 nm) relative to the lamellar period (~25 nm). For the diblock architecture, any chain deformation in the parallel orientation that would stabilize the perpendicular morphology due to nonoptimal thickness in thin films is effectively distributed over many layers in these thicker films.[49]

SCFT calculations for a cylindrical triblock copolymer (Figure 10) predict that the perpendicular configuration is only stable for $\chi_{AW}N \leq 2$. This implies that the range over which the perpendicular orientation is stable is smaller than that for a lamellar triblock copolymer film. As can be seen from the density plot in Figure 12a, when $\chi_{AW}N \leq 2$, the cylinders slightly broaden at the interface in an attempt to wet the surface with the lower γ block. However, for higher $\chi_{AW}N$, the perpendicular orientation does not survive since it costs too much elastic energy to wet the surface with the lower γ midblock which is the minority component. The stable configuration for higher $\chi_{AW}N$ is the presence of a wetting layer of E on the surface with an E−C interface just below that has a roughly sinusoidal oscillation whose period matches that of the underlying E cylinders. Figure 12b shows the density plot for this configuration. A further increase in $\chi_{AW}N$ results in an E wetting layer on the top with a layer of C below it and a completely straight E−C interface. The narrow difference in surface energies for the C and E blocks makes the perpendicular orientation the lower energy state for $CEC_{50.75.10}$. For $CEBC_{60.75.40}$ SFM images show that the cylinders are lying down on the surface of the film. This precludes the possibility of a wetting layer of the E block on the surface and a layer of the C block below it with the E−C interface completely straight. The obtained contrast in SFM would not be possible as the tip would not be able to penetrate through the glassy C phase in order to image the morphology inside the film. In SFM, these oscillations, or half cylinders, appear as lying down cylinders.

A similar conclusion is reached by calculating the looping penalty for $CEC_{50.75.10}$. The calculations suggest that if $\gamma_{PCHE} - \gamma_{PE} < 3$ mJ/m^2, the perpendicular orientation is favored, a criterion that is satisfied by $\Delta\gamma_{C-E}$. As discussed above, a larger difference in surface energies of the two blocks might be able to compensate for this entropy loss and make the parallel orientation energetically more favorable over the perpendicular orientation. For the CEBC triblock copolymer, the decreased surface energy of the EB block due to the higher ethyl branch content containing the larger, nonpolar $-CH_3$ group[43] is able to accomplish this. At 220 °C $\Delta\gamma_{C-EB} \sim 4.7$ mJ/m^2, which is sufficient to compensate for the entropic penalty due to the midblock looping in the wetting layer ($= 3$ mJ/m^2), and hence the parallel orientation with a modulated interface between the top E layer and the underlying C matrix is observed (as predicted

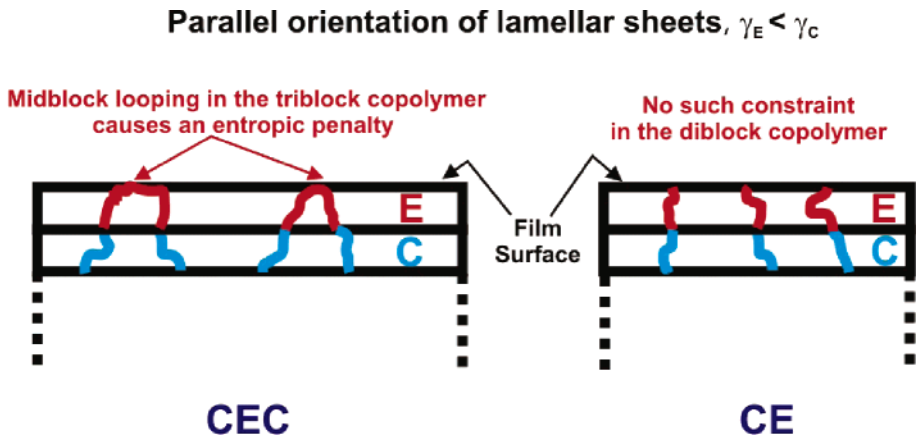

Figure 11. Cartoon depicting the interplay between surface energy and entropy loss due to midblock looping for lamellar block copolymers.

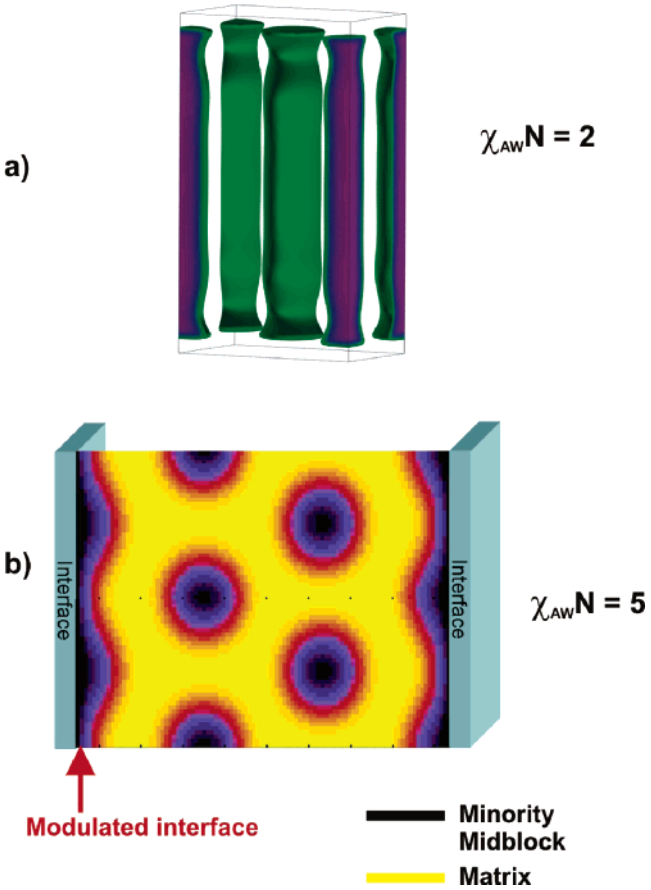

Figure 12. Density plots from SCFT calculations: (a) The 3-D projection of the perpendicular orientation of cylinders at $\chi_{AW}N = 2$. Note the broadening of the cylinder end caps at the interfaces. The elastic strain associated with it stabilizes the parallel orientation at higher values of $\chi_{AW}N$. (b) The 2-D projection of the parallel orientation of cylinders at $\chi_{AW}N = 5$. The wetting layer of the lower surface energy midblock forms a modulated interface with the matrix below it.

from the simulated structure shown in Figure 12b).

Conclusion

In the present work, we have demonstrated the effect of chain architecture and surface energy, γ, on the orientation of microdomains in relatively thick films (~600 nm) of block copolymers of poly(vinylcyclohexane) (C) and poly(ethylene) (E). Spontaneous perpendicular alignment of lamellar and cylindrical triblock copolymers can be obtained if the differences in surface energies ($\Delta\gamma$) of the two blocks is small and the lower surface energy block is incorporated as the midblock. The reason for this behavior is the entropic penalty associated with the midblock looping in the surface wetting layer in the parallel orientation, which is not compensated by a low $\Delta\gamma$. The absence of this constraint stabilizes the parallel orientation in lamellar diblock copolymers. Finally, the range of $\Delta\gamma$ over which this simultaneous perpendicular orientation is observed is lower for the cylindrical block copolymers as compared to the lamellar block copolymers. This is due to the stretching penalties associated with the formation of a wetting layer in the perpendicular orientation as γ for the midblock is reduced further.

Acknowledgment. The authors thank Dr. Nicole Wagner at Dow Chemical for providing us with the P-EB homopolymer and August Bosse for help with the SCFT calculations. We appreciate financial support from NSF DMR Polymers Program Award DMR0307233 and Dow Chemical Co. This work made use of MRL Central Facilities supported by the MRSEC Program of the National Science Foundation under Award DMR05-20415. The use of Advanced Photon Source at Argonne is supported by the U.S. Department of Energy under Contract W-31-109-ENG-38.

References and Notes

(1) Bates, F. S.; Fredrickson, G. H. *Phys. Today* **1999**, *52*, 32.
(2) Matsen, M. W.; Bates, F. S. *Macromolecules* **1996**, *29*, 1091.
(3) Bates, F. S.; Fredrickson, G. H. *Annu. Rev. Phys. Chem.* **1990**, *41*, 525.
(4) Segalman, R. A. *Mater. Sci. Eng. R* **2005**, *48*, 191.
(5) Xu, T.; Kim, H. C.; DeRouchey, J.; Seney, C.; Levesque, C.; Martin, P.; Stafford, C. M.; Russell, T. P. *Polymer* **2001**, *42*, 9091.
(6) Thurn-Albrecht, T.; Steiner, R.; DeRouchey, J.; Stafford, C. M.; Huang, E.; Bal, M.; Tuominen, M.; Hawker, C. J.; Russell, T. P. *Adv. Mater.* **2000**, *12*, 787.
(7) Thurn-Albrecht, T.; Schotter, J.; Kästle, G. A.; Emley, N.; Shibauchi, T.; Krusin-Elbaum, L.; Guarini, K.; Black, C. T.; Tuominen, M. T.; Russell, T. P. *Science* **2000**, *290*, 2126.
(8) Mansky, P.; Liu, Y.; Huang, E.; Russell, T. P.; Hawker, C. J. *Science* **1997**, *275*, 1458.
(9) Sohn, B. H.; Yun, S. H. *Polymer* **2002**, *43*, 2507.
(10) Thurn-Albrecht, T.; DeRouchey, J.; Russell, T. P.; Kolb, R. *Macromolecules* **2002**, *35*, 8106.
(11) Chen, Z.; Kornfield, J. A. *Polymer* **1998**, *39*, 4679.
(12) Hamley, I. W. *J. Phys.: Condens. Matter* **2001**, *13*, R643.
(13) Bates, F. S.; Fredrickson, G. H.; Hucul, D.; Hahn, S. F. *AIChE J.* **2001**, *47*, 762.
(14) Cochran, E. W.; Bates, F. S. *Macromolecules* **2002**, *35*, 7368.
(15) Han, C. D.; Choi, S.; Lee, K. M.; Hahn, S. F. *Macromolecules* **2004**, *37*, 7290.
(16) Richter, D.; Farago, B.; Butera, R.; Fetters, L. J.; Huang, J. S.; Ewen, B. *Macromolecules* **1993**, *26*, 795.
(17) Fetters, L. J.; Lohse, D. G.; Milner, S. T.; Graessley, W. W. *Macromolecules* **1999**, *32*, 6847.

(18) Zhao, J.; Hahn, S. F.; Hucul, D. A.; Meunier, D. M. *Macromolecules* **2001**, *34*, 1737.
(19) Ryu, C. Y.; Ruokolainen, J.; Magonov, S. N.; Hahn, S. F.; Fredrickson, G. H.; Kramer, E. J. *Macromolecules* **2002**, *35*, 2157.
(20) Ruokolainen, J.; Ryu, C. Y.; Magonov, S. N.; Hahn, S. F.; Fredrickson, G. H.; Kramer, E. J. *Macromolecules* **2002**, *35*, 9391.
(21) Hermel, T. J.; Hahn, S. F.; Chaffin, K. A.; Gerberich, W. W.; Bates, F. S. *Macromolecules* **2003**, *36*, 2190.
(22) Lee, B.; Park, I.; Yoon, J.; Park, S.; Kim, J.; Kim, K.; Chang, T.; Ree, M *Macromolecules* **2005**, *38*, 4311.
(23) Hucul, D. A.; Hahn, S. F. *Adv. Mater.* **2000**, *12*, 1855.
(24) Magonov, S. N.; Reneker, D. H. *Annu. Rev. Mater. Sci.* **1997**, *27*, 175.
(25) Brown, G. M.; Butler, J. H. *Polymer* **1997**, *38*, 3937.
(26) Benkoski, J. J.; Flores, P.; Kramer, E. J. *Macromolecules* **2003**, *36*, 3289.
(27) Bashforth, S.; Adams, J. C. *An Attempt to Test Capillary Action*; Cambridge University Press and Deighton, Bell and Co.: London, 1882.
(28) Demarquette, N. R.; Kamal, M. R. *Polym. Eng. Sci.* **1994**, *34*, 1823.
(29) Arashiro, E. Y.; Demarquette, N. R. *Mater. Res.* **1999**, *2*, 23.
(30) Freed, K. F. *Adv. Chem. Phys.* **1972**, *22*, 1.
(31) Helfand, E.; Tagami, Y. *J. Chem. Phys.* **1972**, *56*, 3592.
(32) Hong, Z.; Shaw, M. T.; Weiss, R. A. *Polymer* **2000**, *41*, 5895.
(33) Matsen, M. W.; Schick, M. *Phys. Rev. Lett.* **1994**, *72*, 2660.
(34) Matsen, M. W. *J. Chem. Phys.* **1997**, *106*, 7781.
(35) Helfand, E. *J. Chem. Phys.* **1975**, *62*, 999.
(36) Fredrickson, G. H. *The Equilibrium Theory of Inhomogenous Polymers*; Oxford University Press: New York, 2006.
(37) Cochran, E.; Garcia-Cervera, C. J.; Fredrickson, G. H. *Macromolecules* **2006**, *39*, 2449.
(38) Ceniceros, H. D.; Fredrickson, G. H. *Multiscale Model. Simul.* **2004**, *2*, 452.
(39) Barrat, J. L.; Fredrickson, G. H.; Sides, S. W. *J. Phys. Chem. B* **2005**, *109*, 6694.
(40) Cochran, E.; Garcia-Cervera, C. J.; Fredrickson, G. H. Manuscript in preparation.
(41) Fetters, L. J.; Lohse, D. J.; Richter, D.; Witten, T. A.; Zirkel, A. *Macromolecules* **1994**, *27*, 4639.
(42) Dee, G. T.; Sauer, B. B. *J. Colloid Interface Sci.* **1992**, *152*, 85.
(43) Israelachvili, J. *Intermolecular and Surface Forces*; Academic Press: New York, 1985.
(44) Mansky, P.; Russell, T. P.; Hawker, C. J.; Pitsikalis, M.; Mays, J. *Macromolecules* **1997**, *30*, 6810.
(45) Huang, E.; Russell, T. P.; Harrison, C.; Chaikin, P. M.; Register, R. A.; Hawker, C. J.; Mays, J. *Macromolecules* **1998**, *31*, 7641.
(46) Ten Brinke, G.; Hadziioannou, G. *Macromolecules* **1987**, *20*, 486.
(47) Balsara, N. P.; Tirrell, M.; Lodge, T. P. *Macromolecules* **1991**, *24*, 1975.
(48) De Jeu, W. H.; Lambooy, P.; Hamley, I. W.; Vaknin, D.; Pedersen, J. S.; Kjaer, K.; Seyger, R.; Vanhutten, P.; Hadziioannou, G. *J. Phys. II* **1993**, *3*, 139.
(49) Walton, D. G.; Kellogg, G. J.; Mayes, A. M.; Lambooy, P.; Russell, T. P. *Macromolecules* **1994**, *27*, 6225.

MA0609228